

Ocean Physics Master Report

Marin Ménard

Study of the Amazon plume dynamics in the Northwestern Tropical Atlantic

Key words : Amazon plume, lagrangian particles, mixing, fronts.

Under the supervision of :

Jonathan Gula (jonathan.gula@univ-brest.fr)
Xavier Carton (xcarton@univ-brest.fr)
Pierre L'Hégaret (pierre.lhegaret@univ-brest.fr)

UBO

Université de Bretagne Occidentale



Laboratoire d'Océanographie Physique et Spatiale
Rue Dumont d'Urville
29280 Plouzané

Contents

1	Introduction	1
1.1	Context	1
1.2	The EUREC4A project	2
2	Theoretical contents	2
2.1	Primitive equations	2
2.2	Geostrophic balance	4
2.3	Salinity front and thermal wind	4
2.4	Ekman transport	5
2.5	The Intertropical Convergence Zone (ITCZ)	5
3	Experiments and data used	6
3.1	Data	6
3.1.1	Reanalysis data	6
3.1.2	Climatology	6
3.2	The GIGATL6 simulation	6
3.3	Lagrangian experiment	6
4	Results	8
4.1	Eulerian approach	8
4.1.1	General circulation and seasonal cycle	8
4.2	Plume seasonal variability	9
4.2.1	Extension towards the NECC	9
4.2.2	Salinity	9
4.2.3	Role of the ITCZ	11
4.2.4	NBC retroreflection acceleration	11
4.3	Lagrangian approach	13
5	Conclusion	16
5.1	Summary	16
5.2	Discussion	17
5.2.1	Methods	17
5.2.2	Results	17
5.3	Perspectives	18

Remerciements

Je remercie tout particulièrement Jonathan Gula et Xavier Carton qui m'ont tous les deux beaucoup aidé sur ce stage, mais aussi tout au cours de cette longue année universitaire au contexte bien particulier. Leur disponibilité et leur pédagogie ont permis d'éveiller chez moi une passion pour l'océanographie qui me suivra probablement tout au long de ma vie. Merci aussi à Pierre l'Hégaret qui m'a apporté ses conseils avisés tout au long du stage, et avec beaucoup de patience. Je remercie également Giulia Zerbini, avec qui j'ai travaillé tout au long de l'année qui m'a permis de rester toujours motivé. Enfin, je remercie ma soeur, Maud Ménard, pour m'avoir aidé à réaliser le schéma présenté en figure 5.

Abstract

The Amazon discharge in the Northwestern Tropical Atlantic (NWTA) is the largest in the world, with more than 20 % of the global river discharge. The plume associated to these fresh water masses can be advected in the North Brazil Current (NBC) and its rings, but also by other mesoscale and submesoscale structures like filaments and eddies. The dynamics of this plume is difficult to understand but remains important to describe this singular region. The objective of this internship is to have a better overview of the NWTA dynamics, focusing on the Amazon plume and its interactions with other structures of this region. A CROCO simulation is used with reanalysis data to show the seasonal cycle of the plume. A postprocessing lagrangian experiment has been performed to get information on plume transport and interactions.

1 Introduction

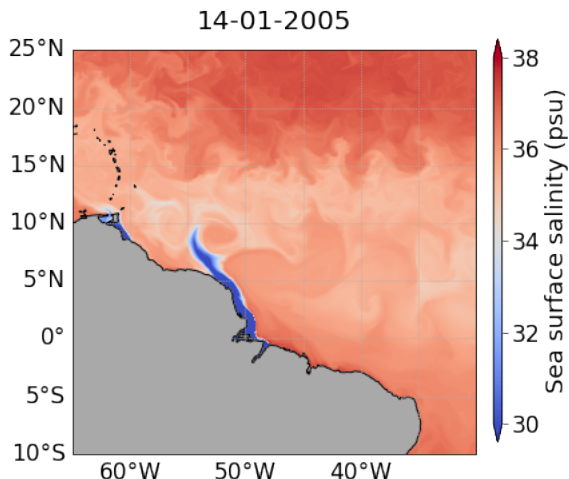


Figure 1: Simulation sea surface salinity in the NWTA on January 14th, 2005. The plume flows northwestward and is advected in a ring of the North.

1.1 Context

With a mean transport of 0.2 Sv [1, 2], the Amazon is the river with the largest outflow in the world. Then, fresh water masses, called plume, spread in the NWTA. Figure 1 shows the sea surface salinity (SSS) in a simulation for an arbitrary day. After being formed on the Brazilian coast, the plume is first advected northwestward through the NBC, which is a western boundary current that follows the continental slope of South America. This current is mainly fed by the South Equatorial Current that splits in two parts offshore from Recife [3]. It carries high-salinity water masses that interact with the Amazon plume. The NBC is a deep current (~ 1500 m) that retroflects on itself around the Demerara plateau. This retroflexion, more intense in summer, creates the NBC rings, whose mean radius is about 130 km, with some rings found beyond 200 km[4, 5]. These anticyclonic rings move northwestward along the continental slope and can vanish when they reach the Antilles, or keep progressing in the Caribbean Sea. They interact with another plume, due to the Orinoco river, whose mean discharge is ~ 0.04 Sv [6], which is approximately 20% of the Amazon's. As the NBC is a deep current, its rings structures can have a strong barotropic component (deeper than ~ 1500 m), but they can also be surface structures whose signature is only visible over a few hundreds meters [7]. Such a signature is probably due to

eddy *cleaving*¹ : deep rings sometimes split at a depth of ~ 200 m, forming two different eddies that move independently, which is very typical of the region [8]. A part of the Amazon plume is trapped and mixed in these rings, but in summer, it can also extend towards the North Equatorial Countercurrent (NECC) through the NBC retroflection. The Orinoco plume, flows exclusively around the Antilles or northwestward to the Caribbean sea, so the only fresh water masses that reach the NECC come from the Amazon.

The seasonal cycle of the general circulation in the NWTA is due to the Intertropical Convergence Zone (ITCZ) variations. It oscillates between 0° and 10°N [9], which implies a change in Ekman transport [10], but also on precipitations. ITCZ oscillations are the main responsible for the Amazon discharge seasonal cycle. Climatology data shows that the discharge is minimum at the end of autumn and starts increasing until May, where it is about 0.25 Sv. El Niño Southern Oscillations (ENSO) are the main factor of the interannual variability of this cycle [11].

The surface velocity in the NBC can reach 1.5 m s^{-1} only 200 km to the Amazon delta. Therefore, salinity fronts in this region can be extremely turbulent. Depending on the Richardson number and the potential vorticity, mixing occurs through Kelvin Helmholtz or symmetric instabilities [12]. It is hard to have relevant satellite measurements to study salinity fronts, as satellite data is often time-averaged over too large periods (1 week or more), and their spatial resolution is too small solve submesoscale structures. Models are strong tools to have information on mixing processes. They are the only way to control the numerous parameters involved. For example, river discharge can be removed to see the influence of the Amazon plume on the NWTA seasonal cycle and frontogenesis [13, 14]. But models are only an idealised way to understand the ocean and represent its dynamics. *In situ* measurements are essential to understand better frontal dynamics, but also to validate model results.

1.2 The EUREC4A project

In this context, the EUREC4A campaign [15] took place in the NWTA at the beginning of 2020. This european measurement campaign involving 4 boats and 4 aircrafts provides (or will provide) large datasets for all kinds of research projects in this region. Some articles have already been published to present the first results of the campaign. It has been shown that the Amazon plume's signature can vary from a few meters to ~ 40 m [16]. When the plume is not mixed (shallow mixed layer), salinity can reach 30 psu close to the brazilian shelf break. Some submesoscale fronts are sharper than 1 psu/km. Strong mixing occurs at these fronts, and their dynamics remains difficult to understand. Section 2 of this work presents the important theoretical contents needed to understand the physical processes discussed. Section 2 of this work presents the important theoretical contents needed to understand the physical processes discussed, starting from the Navier Stokes equation for non specialist readers. Section 3 presents the numerical simulation and the data used in this work. Section 4 presents the important results of the internship, and a discussion of these results is proposed in section 5.

2 Theoretical contents

2.1 Primitive equations

The model used in this report solves the primitive equations in 3D. These are the most general equations used in oceanography. To get them, we start from the Navier-Stokes equations, applied to a fluid in a rotating frame of reference :

$$\rho \left(\frac{\partial \vec{v}}{\partial t} + (\vec{v} \cdot \vec{\nabla}) \vec{v} \right) = -\vec{\nabla}P + \vec{f}_c + \vec{f}_{cf} + \rho \vec{g} + \eta \Delta \vec{v} + \vec{\mathcal{F}} + \vec{\mathcal{D}}, \quad (1)$$

where ρ is the ocean density, \vec{v} is the velocity, $\vec{\nabla}$ is the 3D-gradient operator, P is the pressure, \vec{f}_c is the Coriolis force, \vec{f}_{cf} is the centrifugal force, \vec{g} is the gravitational acceleration, η is the dynamical viscosity, Δ is the Laplace operator, \mathcal{F} represents the other forcing terms, and \mathcal{D} the dissipation ones. As \vec{v} is a 3D-vector, we have 5 variables for 3 equations. To close the problem, we need to add the continuity equations for the density ρ , the salinity S , the temperature T , and the equation of state. It leads to 7

¹This phenomenon has been so called by the authors of [8]

equations for 7 variables :

$$\left\{ \begin{array}{l} \frac{\partial \rho}{\partial t} + \vec{\nabla} \cdot (\rho \vec{v}) = \mathcal{F}_\rho + \mathcal{D}_\rho, \\ \frac{\partial T}{\partial t} + \vec{\nabla} \cdot (T \vec{v}) = \mathcal{F}_T + \mathcal{D}_T, \\ \frac{\partial S}{\partial t} + \vec{\nabla} \cdot (S \vec{v}) = \mathcal{F}_S + \mathcal{D}_S, \end{array} \right. \quad (2a)$$

$$\left\{ \begin{array}{l} \frac{\partial T}{\partial t} + \vec{\nabla} \cdot (T \vec{v}) = \mathcal{F}_T + \mathcal{D}_T, \\ \frac{\partial S}{\partial t} + \vec{\nabla} \cdot (S \vec{v}) = \mathcal{F}_S + \mathcal{D}_S, \end{array} \right. \quad (2b)$$

$$\rho = \rho(T, S, P). \quad (2c)$$

Coordinates system Mesoscale phenomena can be studied in a cartesian frame of reference, as sphericity doesn't play an important role. Then, we set an x -axis pointing eastward, a y -axis pointing northward, and a z -axis pointing in the direction of the Earth radius, from the ocean to the atmosphere. In the following study, every variable will be expressed in this frame of reference. Then, \vec{v} is expressed as (u, v, w) , where u is the zonal velocity, v is the meridional velocity, and w is the vertical velocity.

Reynolds number For mesoscale and submesoscale dynamics in the open ocean, viscosity terms can be completely neglected. Even for length scales of a few kilometers, for strong currents like the NBC with a maximum velocity of 1.5 m s^{-1} , the Reynolds number is around 10^9 . Viscosity becomes important only close to the ocean bottom and at the coast.

Coriolis force The Coriolis force is due to the rotation of the Earth on itself, and is responsible for a lot of planetary, mesoscale and submesoscale phenomena in oceanography, such as eddies, inertial waves, or gyres. We call $\vec{\Omega}$ the Earth's rotation vector. At the latitude ϕ , the Coriolis force is expressed as :

$$\vec{f}_c = \rho \begin{bmatrix} -f^*w + fv \\ -fu \\ f^*u \end{bmatrix}$$

where $f = 2\Omega \sin \phi$ is the Coriolis parameter and where $f^* = 2\Omega \cos \phi$ will be called the reciprocal Coriolis parameter. The vertical component of the Coriolis force is 10^4 times weaker than gravity, so it can be neglected in the z -momentum equation.

Centrifugal force The centrifugal force maximum is reached at the equator, and is equal on Earth to $\rho R_e \Omega^2 \sim 35 \text{ Nm}^{-3}$, where R_e is the Earth radius. Compared to gravity, it is more than 250 times weaker, so the centrifugal force can be neglected.

Incompressible flow The ocean density varies approximately between 1020 kg m^{-3} and 1040 kg m^{-3} . Then, it is reasonable to consider that the studied flows are incompressible, which means that :

$$\partial_x u + \partial_y v + \partial_z w = 0 \quad (4)$$

where " ∂_i " is equivalent to " $\frac{\partial}{\partial i}$ ". This notation is used from here to simplify the reading work.

Equation (4) can be scaled to determine the relative importance of each term. Let $L \sim 60 \text{ km}$ be the horizontal length scale, $H \sim 3 \text{ km}$ the vertical length scale, $U \sim 1 \text{ m s}^{-1}$ the horizontal velocity scale, and W the vertical velocity scale.

$$\frac{W}{H} = \frac{U}{L} \Rightarrow W \sim 0.05 U \quad (5)$$

Incompressibility combined with the thinness of the ocean at mesoscale leads to weak vertical velocities. Scaling of equation (1) leads to :

$$\left\{ \begin{array}{l} \rho(\partial_t u + u \partial_x u + v \partial_y u + w \partial_z u - fv) = -\partial_x P + \mathcal{F}_x + \mathcal{D}_x \\ \rho(\partial_t v + u \partial_x v + v \partial_y v + w \partial_z v + fu) = -\partial_y P + \mathcal{F}_y + \mathcal{D}_y \end{array} \right. \quad (6a)$$

$$\left\{ \begin{array}{l} \rho(\partial_t v + u \partial_x v + v \partial_y v + w \partial_z v + fu) = -\partial_y P + \mathcal{F}_y + \mathcal{D}_y \\ 0 = -\partial_z P - \rho g \end{array} \right. \quad (6b)$$

$$0 = -\partial_z P - \rho g \quad (6c)$$

Equation (6c) is now a balance, called hydrostatic balance, between the pressure gradient and the gravity force. We can notice that thanks to equation (5), a part of the zonal component of the Coriolis force has been neglected. The reciprocal Coriolis parameter is therefore no longer present in the equation, which explains why it doesn't have a traditional name.

Boussinescq approximation As variations of density are small compared to the mean value ρ_0 , we can make the Boussinescq approximation, which consists in neglecting the variations of ρ , except in the z -momentum equation. This classical approximation enables important simplifications of the momentum equations. The initial set of equations becomes :

$$\left\{ \begin{array}{l} \partial_t u + u \partial_x u + v \partial_y u + w \partial_z u - fv = -\frac{1}{\rho_0} \partial_x P + \mathcal{F}'_x + \mathcal{D}'_x \\ \partial_t v + u \partial_x v + v \partial_y v + w \partial_z v + fu = -\frac{1}{\rho_0} \partial_y P + \mathcal{F}'_y + \mathcal{D}'_y \end{array} \right. \quad (7a)$$

$$0 = -\frac{1}{\rho_0} \partial_z P - \frac{\rho}{\rho_0} g \quad (7c)$$

$$\left\{ \begin{array}{l} \frac{\partial \rho}{\partial t} + \vec{\nabla} \cdot (\rho \vec{v}) = \mathcal{F}_\rho + \mathcal{D}_\rho, \\ \frac{\partial T}{\partial t} + \vec{\nabla} \cdot (T \vec{v}) = \mathcal{F}_T + \mathcal{D}_T, \end{array} \right. \quad (7d)$$

$$\left\{ \begin{array}{l} \frac{\partial S}{\partial t} + \vec{\nabla} \cdot (S \vec{v}) = \mathcal{F}_S + \mathcal{D}_S, \\ \rho = \rho(T, S, P). \end{array} \right. \quad (7e)$$

$$(7f) \quad (7g)$$

where $\mathcal{F}'_i = \frac{1}{\rho_0} \mathcal{F}_i$ and $\mathcal{D}'_i = \frac{1}{\rho_0} \mathcal{D}_i$. These equations, called primitive equations, are the equations solved by the CROCO model used in this work, and detailed in section 3.2.

2.2 Geostrophic balance

Mesoscale circulation respects at first order the geostrophic balance. At this length scale, the Rossby number $Ro = \frac{U}{fL} \sim 0.1$ is small, which enables to neglect the advection terms. For a stationary state, and without forcing or diffusion, the pressure gradient balances the Coriolis force on the horizontal, and the gravity on the vertical :

$$\left\{ \begin{array}{l} -fv = -\frac{1}{\rho_0} \partial_x P \\ fu = -\frac{1}{\rho_0} \partial_y P \end{array} \right. \quad (8a)$$

$$\left\{ \begin{array}{l} -fv = -g \partial_x \zeta \\ fu = -g \partial_y \zeta \end{array} \right. \quad (10a)$$

$$\left\{ \begin{array}{l} -fu = -g \partial_y \zeta \\ fv = -g \partial_x \zeta \end{array} \right. \quad (10b)$$

These equations are called geostrophic balance and they probably represent the most useful set of equations to explain mesoscale circulation. If we approximate ρ to its mean value ρ_0 and integrate the hydrostatic balance (7c), we get :

$$P(x, y, z, t) = P_{\text{atm}} - \rho_0 g(z - \zeta(x, y, t)) \quad (9)$$

where P_{atm} is the atmospheric pressure at the surface of the ocean and ζ is the free surface. This expression can be used to rewrite the geostrophic balance with free surface instead of pressure gradient :

$$\left\{ \begin{array}{l} -fv = -g \partial_x \zeta \\ fu = -g \partial_y \zeta \end{array} \right. \quad (10a)$$

$$\left\{ \begin{array}{l} -fu = -g \partial_y \zeta \\ fv = -g \partial_x \zeta \end{array} \right. \quad (10b)$$

Thanks to these equations, altimetry can be related to surface currents, called geostrophic currents. These currents are a good first order approximation to real mesoscale currents.

2.3 Salinity front and thermal wind

The Amazon represents a large discharge of fresh water in the ocean. This is why the NWTA presents sharp mesoscale and submesoscale salinity fronts. To understand the dynamics of the region, it is important to remind the main processes involved in this kind of fronts. At first order, density is driven by temperature. In the NWTA region, temperature variations are small, but salinity varies much more because of tropical rains and river discharge. Thus, we can consider that density variations are then more due to salinity than temperature. Salinity fronts are then also density fronts. Velocity shear can be related to the density gradient. By taking the z -derivative of the geostrophic balance, and replacing the pressure gradient thanks to the hydrostatic balance, we get :

$$\left\{ \begin{array}{l} \partial_z v = -\frac{g}{\rho_0 f} \partial_x \rho \\ \partial_z u = +\frac{g}{\rho_0 f} \partial_y \rho \end{array} \right. \quad (11a)$$

$$\left\{ \begin{array}{l} \partial_z v = -\frac{g}{\rho_0 f} \partial_x \rho \\ \partial_z u = +\frac{g}{\rho_0 f} \partial_y \rho \end{array} \right. \quad (11b)$$

We can deduce from these equations that a density front (thus a salinity front) generates a jet, parallel to the front, travelling with the denser (saltier) water masses on its right in the Northern hemisphere, and on its left in the Southern hemisphere. Nevertheless, this result is true only if velocity goes to zero at some depth, which is the case in the NWTA region. If we assume that velocity is null around $H = 100$ m, and for a sharp density front of 0.1 psu/km, a scaling of equations 11 gives a velocity of $U \sim 1 \text{ m s}^{-1}$, which is comparable to the NBC surface velocity.

2.4 Ekman transport

The Ekman transport is a well-known concept in oceanography. It has been developed by Vagn Walfrid Ekman, a Swedish oceanographer. It states that the main water transport due to wind stress is at 90° right/left to the wind in the Northern hemisphere/Southern hemisphere. This result is gotten from the primitive equations in a steady state and at mesoscale ($Ro \ll 1$). Considering only a mechanical forcing from the atmosphere (no heating) and no pressure gradients, equations (7a) and (7b) become :

$$\left\{ \begin{array}{l} -fv = \frac{1}{\rho_0} \partial_z \tau_x \\ fu = \frac{1}{\rho_0} \partial_z \tau_y \end{array} \right. \quad (12a)$$

$$\left\{ \begin{array}{l} -fM_y = \tau_x \\ fM_x = \tau_y \end{array} \right. \quad (12b)$$

where τ_x and τ_y are respectively the wind stress in the zonal and meridional directions. To get the transport induced by wind, we suppose that the wind effects are negligible below a certain depth, called h_{ek} . After multiplying them by ρ_0 , the previous equations can be integrated between the surface and this depth :

$$\left\{ \begin{array}{l} -fM_y = \tau_x \\ fM_x = \tau_y \end{array} \right. \quad (13a)$$

$$\left\{ \begin{array}{l} -fM_y = \tau_x \\ fM_x = \tau_y \end{array} \right. \quad (13b)$$

where $M_x = \int_0^{h_{ek}} \rho_0 u dz$ and $M_y = \int_0^{h_{ek}} \rho_0 v dz$ are respectively the vertically-integrated transports induced by wind in the zonal direction (eastward if $M_x > 0$) and in the meridional circulation (northward if $M_y > 0$). In the first half of the 20th century, Fridtjof Nansen, a Norwegian oceanographer and explorer² observed during a North pole expedition that icebergs were not moving in the wind direction, but with an angle of 20° to 40° to the right. Ekman wanted to understand what could explain this curiosity. If we consider a wind blowing eastward in the Northern hemisphere, τ_x is positive, f is positive, so M_y is negative. Then, a westerly wind generates a main Ekman transport southwestward, 90° right to the wind stress. As 9/10 of an iceberg volume is submerged, it is subject to both wind stress and current stress, which are not in the same direction because of the Coriolis force. It explains why icebergs are drifting with such an angle. Thanks to this theory, Ekman allowed to better understand wind-induced phenomena, such as drifters dynamics, coastal or equatorial upwellings.

2.5 The Intertropical Convergence Zone (ITCZ)

In the Equatorial Atlantic, winds are mainly blowing westward for both hemispheres. To cross the Atlantic from Europe, sailors are used to go southward first, following the African coast, before making a right turn westward around the Canaries Islands, where trade winds push ships towards Antilles and then America. As the first navigators using this pathway were part of the “triangular trade”, these low latitude winds have been called “trade winds” in English, and it is still the case nowadays. These winds can be explained by the presence of convection cells, called “Hadley cells”, at low latitudes (between $\sim 0^\circ$ and $\sim 30^\circ$). At the equator, as the ocean and the lower atmosphere are both warm, and as the tropopause is cold ($\sim -20^\circ\text{C}$), the atmosphere is unstable. Warm air of the surface starts moving upward. As it takes altitude, the vapor pressure of the air decreases, and clouds are formed. This is why we can observe around the equator large stormy and rainy clouds with mushrooms shapes. Then, because the air moving upward creates an excess of pressure at the equator, equatorial air masses start moving poleward. At $\sim 30^\circ$, these air masses start moving downward³, which creates large stable anticyclones (high pressure), such as the Azores or Saint Helena anticyclones. To close the cell, surface winds have to blow equatorward between 0° and 30° . but because of the Coriolis force, they are deviated to the left in the Southern hemisphere, and to the right in the Northern hemisphere. Thus, low latitude winds blow southwestward in the Northern hemisphere, and northwestward in the Southern hemisphere. Hadley cells can be seen as Rayleigh Taylor instability

²Actually, Fridtjof Nansen is much more than that. He's also a Nobel Peace Prize laureate and a zoologist. Curious readers can refer to his long biography for more information.

³This downward movement around 30° is due to the conservation of angular momentum.

cells, but in a rotating frame. Also, they are subject to seasonal variability. In winter, as the meridional temperature gradient increases, the cell becomes stronger, and moves equatorward. Because of this, the zone between the two cells, called ITCZ, moves northward during the Northern summer (around 10°N), and southward during the Southern summer (around 0°). In this zone, trade winds vanish, and the only wind that blows is due to storms. On the lands, ITCZ movements determine wet and dry seasons.

3 Experiments and data used

This part presents the different simulations and data used for the results detailed in section 4

3.1 Data

3.1.1 Reanalysis data

The Simple Ocean Data Assimilation (SODA) has been used to compare and validate model results at the surface. **It has also been used for the atmospheric forcing of the GIGATL6 simulation.** Reanalysis data like SODA provides information on the ocean thanks to measurements combined with numerical simulations. As *in situ* measurements are inequally spread over the ocean, models provide information where it is missed. It is important to notice that the SODA dataset does not deliver salinity at the surface, but 5 m below. We will by default consider that the salinity doesn't change much over 5 m, and we will assimilate salinity at 5 m to SSS. For the atmospheric forcing, the temporal resolution is 1 h, which is larger than the simulation time step, so a linear interpolation of the data is made at each time step.

3.1.2 Climatology

The In Situ Analysis System (ISAS) has been used as climatology data for salinity. This dataset is computed from Argo float measurements on a regular grid thanks to an optimal interpolation method. The Argo floats drift at ~ 1000 m before making CTD (conductivity, temperature and depth) profiles between 0 m and 2000 m. With 6 different depths between 0 m and 20 m, ISAS's vertical resolution is better than SODA's, so it has been chosen to get information on the vertical structure of the plume.

3.2 The GIGATL6 simulation

The GIGATL6 simulation⁴ has been performed in the whole Atlantic thanks to the Coastal and Regional Ocean CCommunity model (CROCO, www.croc-ocean.org), that solves numerically the primitive equations detailed in section 2.1. The grid is a non-squared grid illustrated on figure 2, with a orizontal resolution and 50 vertical sigma levels (see figure 14 for more details). Boundary conditions are set to be a "no-slip" condition at the coast, which means that all the velocities are set to zero. At the bottom of the ocean, a free-slip condition with a parametrised frictionnal drag is set. Atmospheric forcing has been chosen to be reanalysed meteorology data. Tides effects are not studied here, so tides have been removed from the simulation. Sources points of water at 10 psu have been set to simulate the Amazon inflow. Their temperature and flow rates are computed thanks to a linear interpolation in time of monthly climatology data. Locations of the sources and their flow rates are detailed on figure 3.

3.3 Lagrangian experiment

To get information on transport and mixing, two different postprocessing experiments with lagrangian particles have been performed. They have been made from the GIGATL6 simulation, whose outputs are every 12 hours. The first one, LAG-2D-6KM, uses particles that can move only at the surface. The second one, LAG-3D-6KM enables particles to move on the vertical. The particles trajectories have been computed thanke to the Pyicles code⁵. This code uses an order 4 Runge-Kutta scheme. Particles are initiated every week downstream to the Amazon delta. They are uniformly spread each 3 km. Tocantins river discharge is neglected since it represents less than 10% of the total discharge. The time step has been chosen to respect the Courant Friedrich Levy criterion⁶.

⁴More information on <https://github.com/Mesharou/GIGATL>

⁵More information on <https://zenodo.org/record/4973786.YR9qNNMzbMI>

⁶This criterion states that the information can't cross more than one grid cell in a time step. If Δt is the time step, U_{\max} the maximum velocity of the simulation and Δx the spatial step of the grid, the CFL condition is $\Delta t \leq \frac{\Delta x}{U_{\max}}$

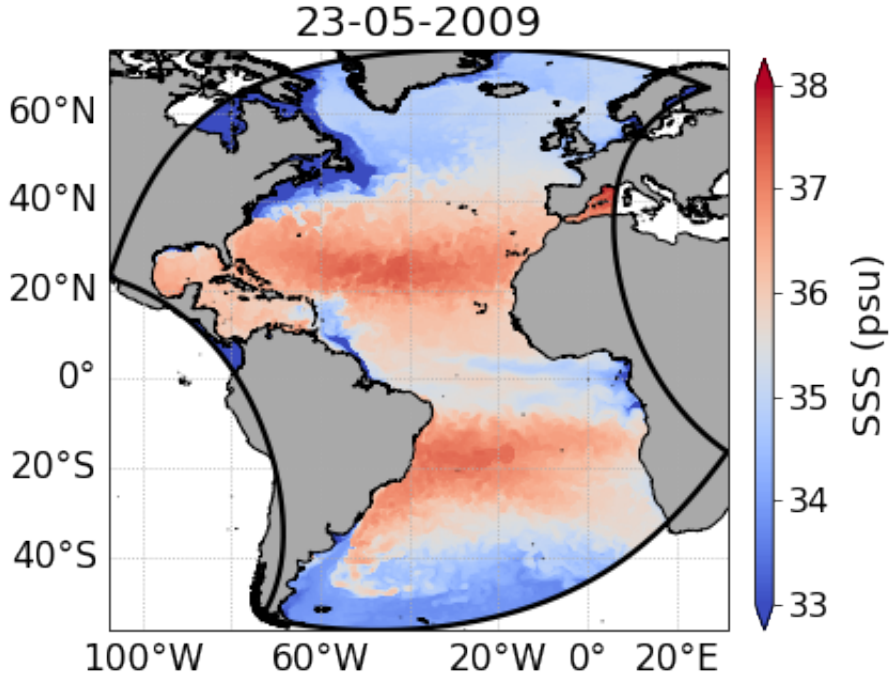


Figure 2: SSS in the GIGATL6 simulation on May, 23rd. The grid's limits are represented with the black thick lines.

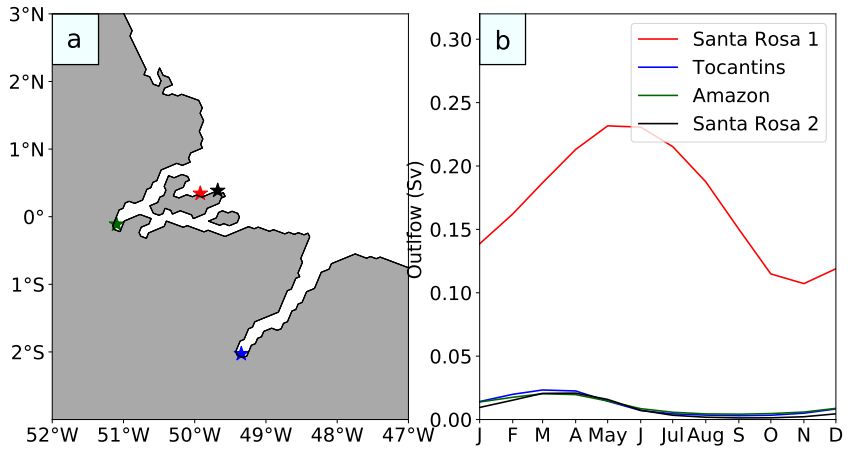


Figure 3: Fresh water sources locations (a) and discharges associated (b). Names are arbitrarily chosen considering their locations. Discharges are given by climatology data.

For the 2D simulations, the line of particles is at the surface, but for the 3D one, it has been decided to superpose 4 different lines. As the model used is made for open ocean, coastal topography is not well represented. Depths shallower than 20 m are set to 20 m. The line of particles has been chosen to be over a 20 m-isobath. With such a configuration, illustrated in figure 4, particles are on a regular grid. The objective of this experiment is to associate to each particle a certain volume of Amazon fresh water. Two different ways have been chosen to calculate the volume. Let us call $\Delta t = 1$ week the time between two releases of particles. The first one consists, for each particle release, in dividing the volume of Amazon water that came in the ocean in a time Δt by the number of particles released in a row. It can be

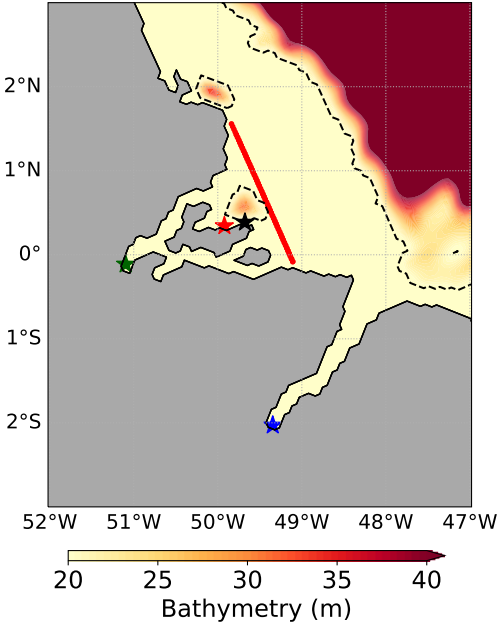


Figure 4: Background color represents the bathymetry, the dashed line is the 20 m-isobath, the stars are the fresh water sources of the GIGATL6 simulation, the red dots represent the particles initial location, which is above a uniform topography of 20 m.

summarized as :

$$V_j = \frac{\bar{q}_j \Delta t}{N_p} \quad (14)$$

where V_j is the volume of the j^{th} particle, N_p is the number of particles released in a row, \bar{q}_j is the mean Amazon discharge over a period Δt , at the time where the j^{th} particle is released. With this first approach, the seasonal variability of the Amazon inflow is taken in account. For example, particles released in June represent a larger volume than the ones released in December. But this method doesn't consider the velocity field where particles are released. The second one, more complex, but also closer to a real fluid mechanics approach, takes in account the velocity at each point of the release. To explain this method, we call $u_{k,l}$ the transversal velocity at the k^{th} point of the l^{th} line, and $V_{k,l}$ its volume. We can compute $V_{k,l}$ as :

$$V_{k,l} = \delta y \delta z \Delta t \bar{u}_{k,l} \quad (15)$$

where $\delta y / \delta z$ is the meridional/vertical length occupied by each particle (see figure 5), and $\bar{u}_{k,l}$ is the temporal mean of $u_{k,l}$ over a period of Δt , at the time where the particle (k, l) is released. With such a formula, the discharge temporal variability is taken in account through the variations of $u_{k,l}$, but also the spatial variations of velocity.

4 Results

4.1 Eulerian approach

4.1.1 General circulation and seasonal cycle

GIGATL6 mean surface currents over 8 years of simulation in the NWTA region are shown in figure 6. The total year is separated in four 3-month-periods : winter between January and March (JFM), spring between April and June (AMJ), summer between July and September (JAS), and autumn between October and December (OND). The NBC flows northwestward along the continental slope, with a surface velocity of $\sim 1 \text{ m s}^{-1}$, and retroflects around the Demerara plateau. This retroreflection forms rings that detach from the plateau and that start moving northwestward before reaching the Antilles in ~ 2 months. As this time is short compared to the average time, we can't observe directly these rings, but it is clear that the NBC loses a part of its kinetic energy after the plateau, as a part of it has been transferred to the rings. Figure 6 shows also important seasonal variations. The NBC and its retroflection get more

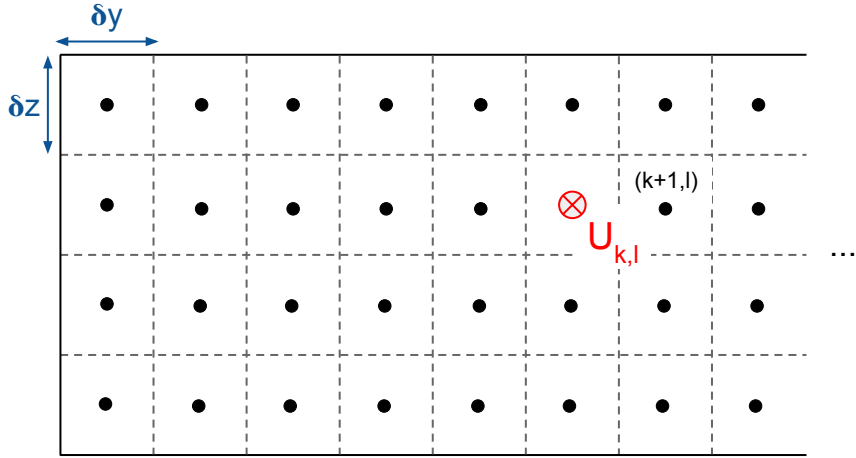


Figure 5: Illustration of a release of particles viewed from the Amazon delta. Particles are represented with the black dots and indexed with (k, l) , k representing the columns, l the lines. Each one represents a surface $\delta y \delta z$ corresponding to the dashed-line grid. Transversal velocity $u_{k,l}$ is illustrated with the red vector. Each week of the LAG-3D-6KM simulation, 208 particles (52 columns) are released in this configuration.

intense in summer, which intensifies also the NECC. This seasonal current flows eastward and is the only way for plume waters to travel in this direction. It is located around 6°N and is active in summer and autumn, as observed by drifting buoys and ships [17].

4.2 Plume seasonal variability

4.2.1 Extension towards the NECC

The first step of this work has been to observe the SSS in GIGATL6. It has been noticed that most of the fresh water masses of the Amazon were travelling northwestward towards the Antilles or were stuck at the coast. But at the end of summer, a part of the plume gets to the NECC. Figure 7 shows this event in 2006. It is observed every year of the simulation, but also by satellite measurements, which is essential to validate the model and the conclusions made thanks to it. The first image illustrates the plume behavior during the largest part of the year, except that the retroflection is less intense in winter (a). Thus, a ring detaches from the retroflection, which loses intensity (b) as it has transferred most of its kinetic energy to the ring. The NBC starts then retroreflecting again close to the ring, creating a strong horizontal shear that mixes the plume (c). As no ring is formed afterwards, the plume extends towards the NECC, which reduces the SSS of ~ 0.5 psu in the region (d).

4.2.2 Salinity

To go further, 3 boxes illustrated on figure 7d have been defined in the NWTA. The first one, called “A” for “Antilles”, is the box where most of the plume water masses get to. The second one, called “NECC”, is located around the origin of the NECC, which can be reached by the Amazon plume at the end of summer. The last one, called “R” for “retroflection”, is located at the NBC retroflection, as it is the transition region where plume waters go through before getting to the NECC. These boxes are represented in figure 7d with the SSS on January 14th, 2005 as background, and details on their locations are shown in table 1.

Box	Minimum latitude	Maximum latitude	Minimum longitude	Maximum longitude
Antilles	7.5°N	17.5°N	61°W	53°W
NECC	2.5°N	12.5°N	48°W	37°W
Retroflection	3°N	9°N	53°W	45°W

Table 1: Coordinates of the three boxes illustrated on figure 7d.

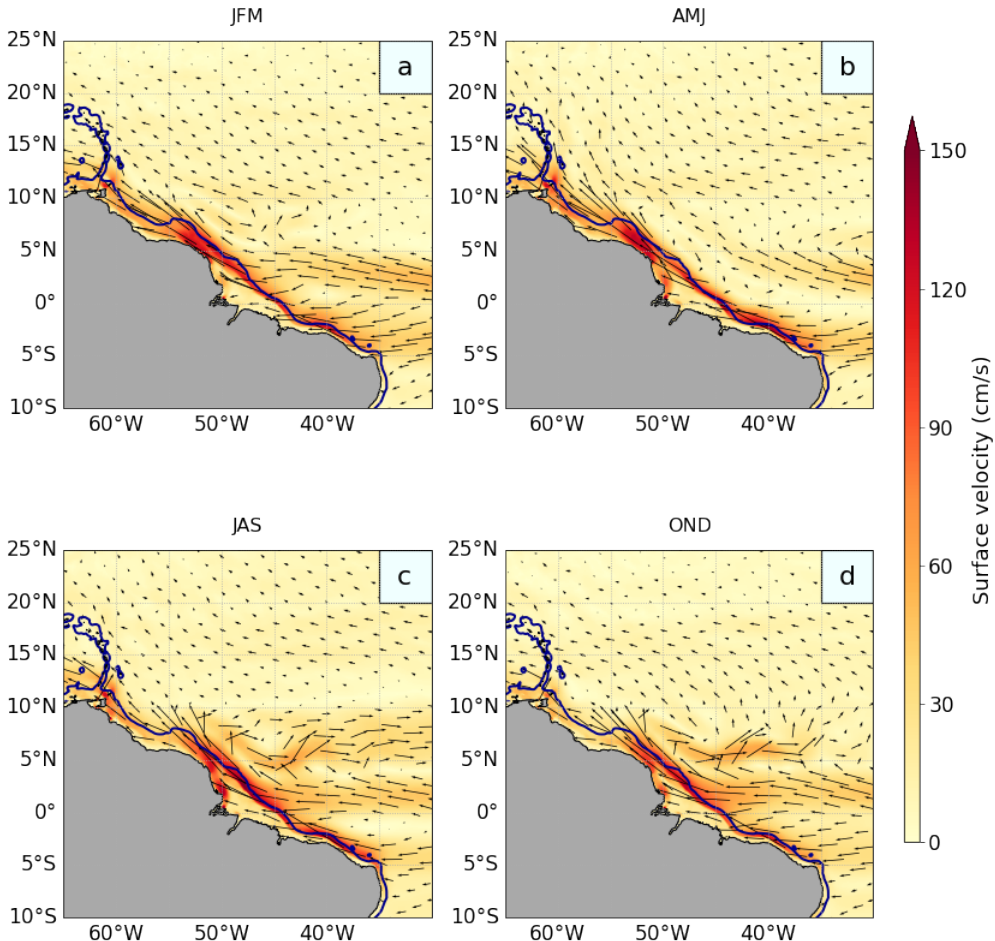


Figure 6: Mean surface currents over 8 years in the GIGATL6 simulation for winter (JFM), spring (AMJ), summer (JAS) and autumn (OND). Black arrows correspond to the current direction. Continental slope is shown with the blue line representing the 1000 m-isobath.

Because plume waters are essentially located in the upper 20 m ocean, it is possible to have a first overview of the plume dynamics by looking at the SSS in the different boxes. Figure 8 presents the annual mean SSS over the 3 different boxes. It has been computed over 7 complete years, from 2005 to 2011. Thick lines represent the results for the GIGATL6 simulation, and dotted lines represent the results obtained from the reanalysis data (see section 3.1.1). It is clear that the model delivers a good idea of the real dynamics, as variations of salinity happen at the same time, except around the Antilles. SSS decreases of ~ 2 psu for both model and reanalysis, but in different times : from April to July in the model, and from April to mid-August in reanalysis. At this period, the flow rate of the Amazon increases, and the plume flows northwestward along the coast or is advected in NBC rings. More fresh water reaches the Antilles before being completely mixed, which explains the SSS falling in both cases. The retroflection mean SSS also starts decreasing when the Amazon outflow increases. The plume keeps being stuck at the coast for ~ 3 months. Then, it starts being advected in the retroflection which leads it to the NECC. The SSS decreases between August and September in this box because of this event (see figure 7).

Models have the important advantage of giving information at depth too. Figure 9 shows the evolution of the mean salinity in the three different boxes over 20 m. As CROCO models use sigma coordinates, salinity is first computed by cubic interpolation on a regular grid of 10 layers between 0 m and 20 m, before taking the mean value over the three spatial axes. Results of the GIGATL6 simulation are then compared to climatology data (see section 3.1.2), represented with dots. Same trends are observed between figures 8 and 9, but the range of values is smaller. This was expected considering that the salinity varies more at the surface than at 20 m, where the plume is much more mixed. This can come from the mixed layer parametrization, or from differences between stratification in the model and in reality, as the model SSS

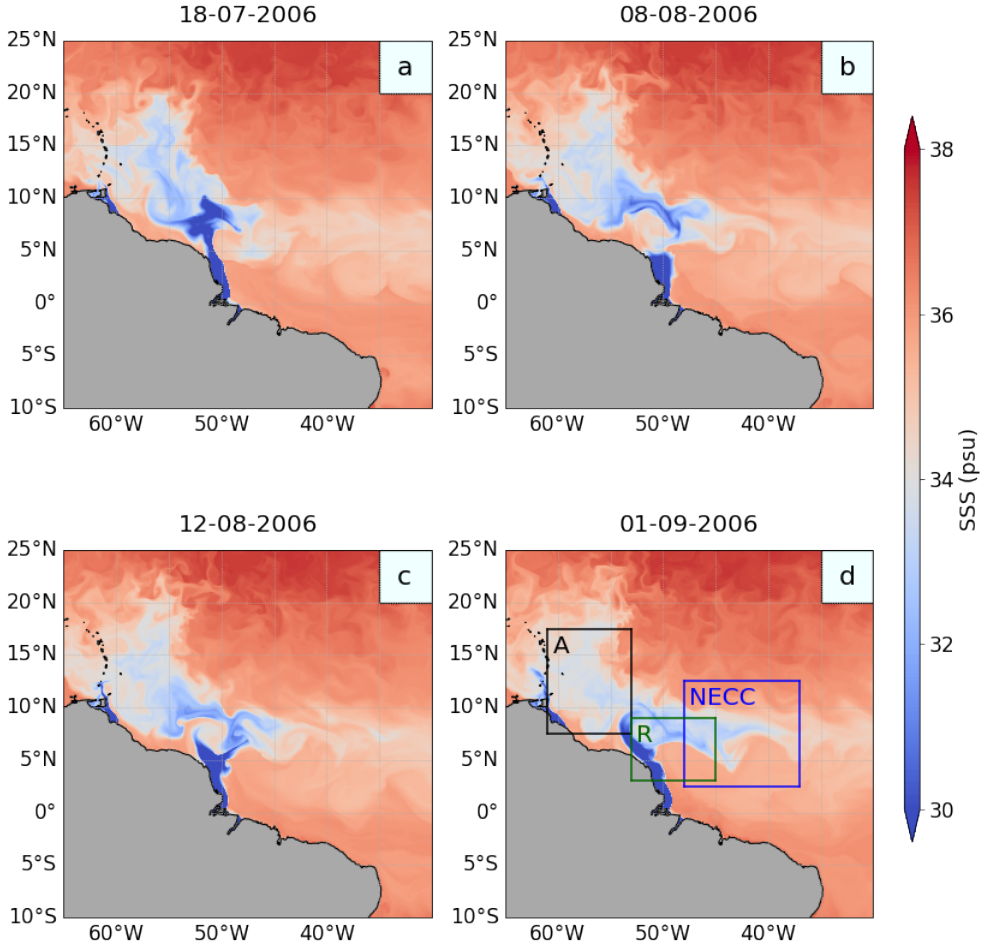


Figure 7: SSS at 4 different days in summer. The plume is rolling around the NBC retroflection (a). A ring is then formed and the plume is advected and mixed (b). The ring detaches from the retroflection, which becomes intense south to the ring (c). The plume is advected in the retroflection and reaches the NECC (d).

is quite close to the ISAS data. The difference is in the order of the salinity gap induced by the plume, which is problematic to get to more quantitative conclusions.

4.2.3 Role of the ITCZ

An 8-year mean of the surface winds used in the GIGATL6 simulation is presented in figure 10. The ITCZ variability is clear, since the minimum wind velocity is around 10°N for the months of July, August and September, and around 0° for the months of January, February and March. Because of this, winds blow on-shore on the Southeastern American coast, except in summer⁷, where trade winds of the Southern Hadley cell blow along the coast. The Ekman transport (see section 2.4) in summer is then offshore, which enables a part of plume waters to get to the NECC. In the rest of the year, the Ekman transport is mostly northwestward, in the direction of the NBC, so most of the plume waters are advected in the NBC or stuck at the coast.

4.2.4 NBC retroflection acceleration

To explain why a part of the plume can reach the NECC, it is important to be more precise on the role of the NBC retroflection. The plume reaches this region and the part of it that is advected in the retroflection is then trapped in the NBC rings. But in July, a ring detaches, which enables the plume to roll around the retroflection before reaching the NECC. From this, two different hypotheses are possible

⁷To simplify the purpose, “summer” and “winter” will designate by default summer and winter of the Northern hemisphere.

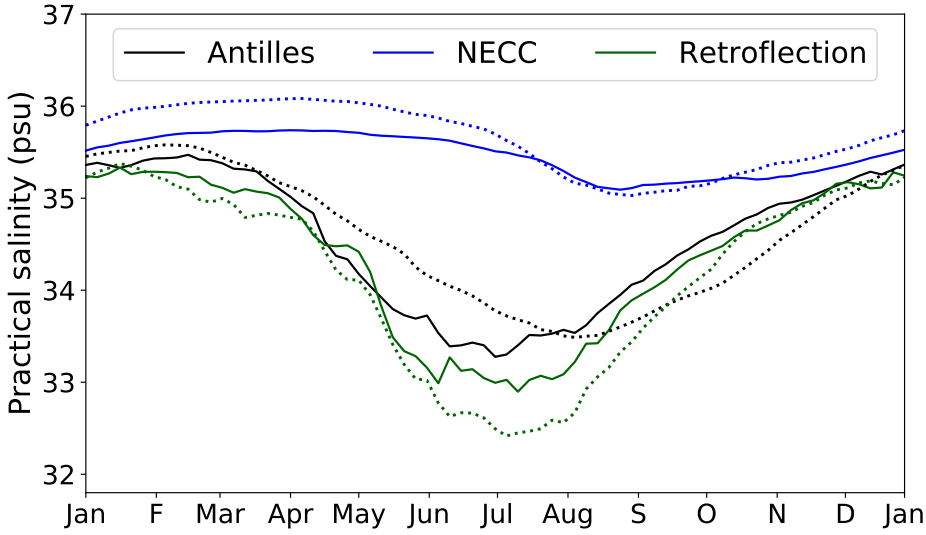


Figure 8: Mean SSS over boxes "Antilles" (black), "NECC" (blue) and "Retroflection" (green) in the GIGATL6 simulation (thick lines) and 5 m-depth salinity from ISAS data (dashed line).

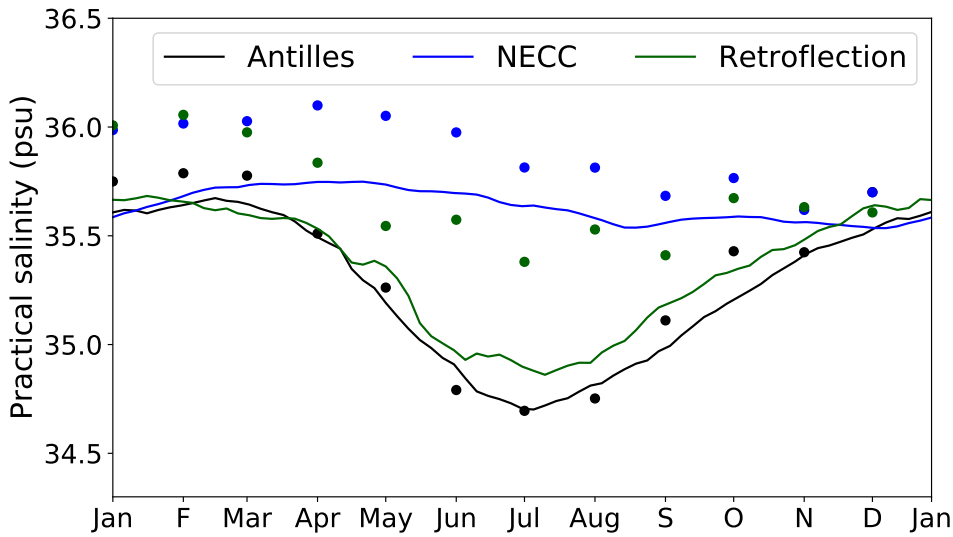


Figure 9: Mean salinity over 20 m in GIGATL6 (thick line) and climatology data (dots).

to explain why the plume can cross the retroflection : 1°) NBC rings are lately formed after July 2°) The retroflection accelerates at the beginning of summer. The first one has not been investigated as it was more dedicated to Loïc Eisenring's internship, another student working at the LOPS.

Figure 11 shows the annual mean of surface kinetic energy (SKE) integrated over the different boxes, from 2005 to 2011 (7 years) in the GIGATL6 simulation. The increase of kinetic energy in the retroflection region is directly linked to the increase in the NECC region, corresponding to the birth of the NECC. The retroflection starts accelerating between May and June and its SKE reaches its maximum in August. Several factors are responsible for this acceleration. First of all, the ITCZ is moving northward during this period, so northwestward Ekman transport decreases, and more water can be advected offshore. A second factor, and maybe the main one, is the Amazon outflow. As shown in figure 3, its maximum is reached between May and June. During this period, water accumulates on the left side of the NBC. According to the geostrophic balance (10), the NBC is supposed to be less intense. This behavior is not

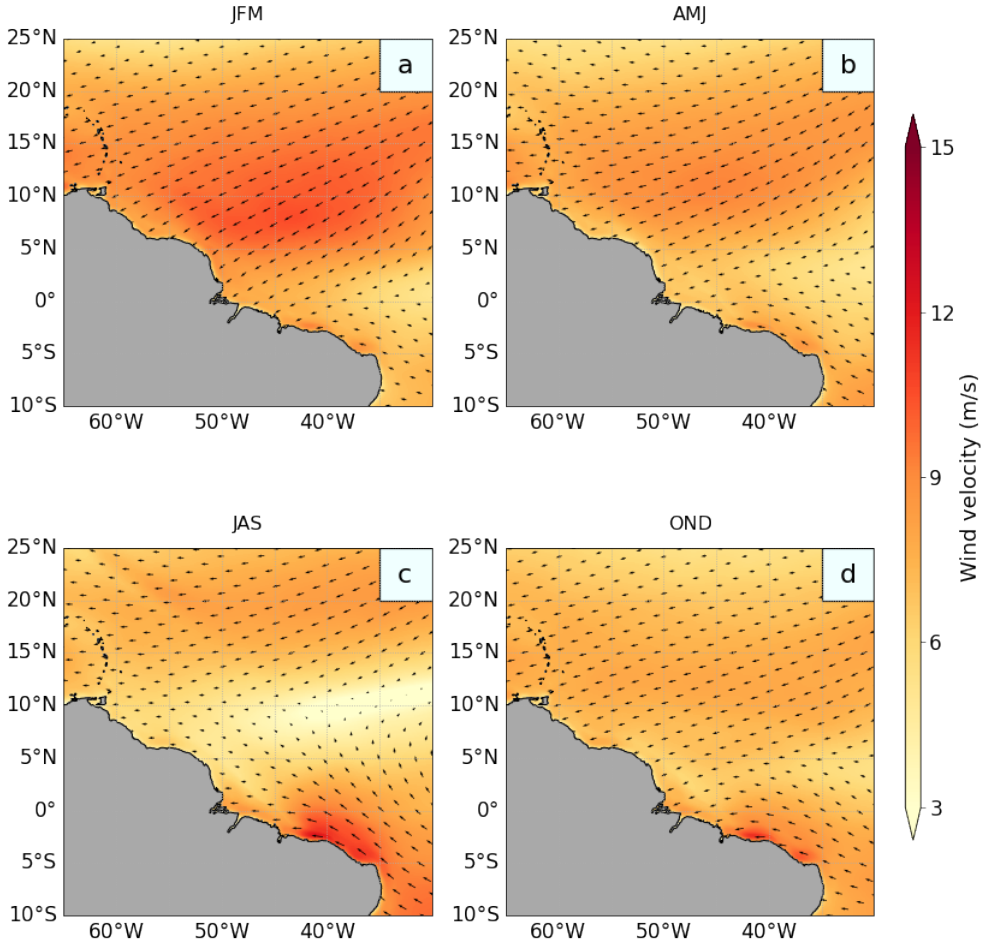


Figure 10: Wind velocity 10m above the surface in the GIGATL6 simulation for winter (JFM), spring (AMJ), summer (JAS) and autumn (OND). Background represents the wind intensity, and black arrows its direction. Wind stress is given by reanalysis data (see section 3.1.1) and velocity is computed thanks to [18]. The minimum intensity corresponds to the ITCZ position that oscillates between $\sim 0^\circ$ and $\sim 10^\circ\text{N}$.

very clear in figure 6, but the NBC surface velocity decreases of $\sim 25 \text{ cm s}^{-1}$ between April and June (see figure 15). This dynamical feature has been detailed in [14]. Then, the Amazon outflow starts decreasing, and fresh water accumulated around the delta is advected northwestward. This creates a sharp mesoscale salinity front. This salinity front, according to section 2.3, creates a jet that accelerates the NBC. The plume is then advected on the external side of the retroflection, which contributes to accelerate it too.

4.3 Lagrangian approach

To have more quantitative information on transport in the region, a postprocessing lagrangian experiment has been performed (see section 3.3 for details). Two different methods have been chosen to associate to each particle a certain volume of Amazon water (see section 3.3). The second one, corresponding to equation (15), is supposed to give more realistic results, as it considers the velocity profile at the Amazon delta. Figure 12 represents the volume computed from this equation. It actually shows that results gotten from this method are too discontinuous to be considered as meaningful results. Our fear of finding negative volumes appears also to be legitimate. So it has been chosen not to go further with this method, however better it seemed to be at the beginning of the work. From here, every volume associated to particles is computed from equation (14), and will be called lagrangian volume. Figure 13 shows several temporal series of the lagrangian experiments described in section 3.3. The two first series represent the volume computed from equation 14 for the 2D (a) and 3D (b) experiments. Subfigure (c) represents the volume of water fresher than 35 psu (called eulerian volume) in the different boxes – this value has been chosen to be consistent with [16]. Subfigure (d) shows the precipitation rate used for the GIGATL6 simulation integrated over the different boxes, and subfigure (e) presents the SKE integrated

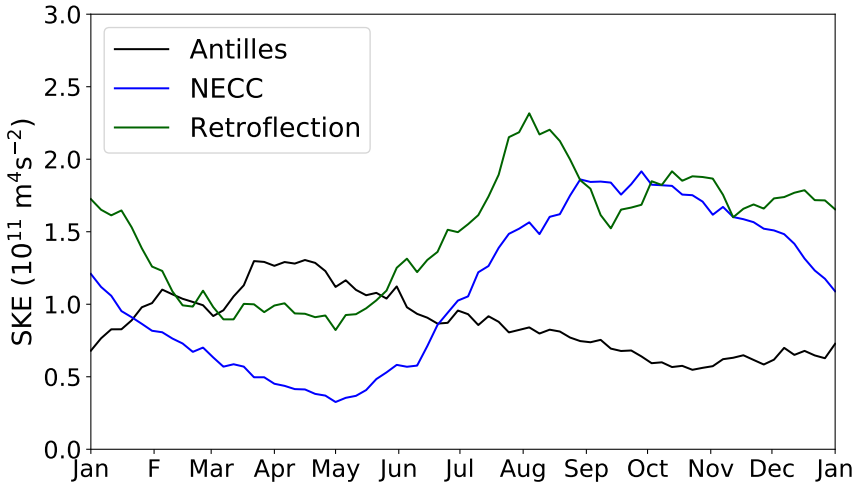


Figure 11: Annual mean from 2005 to 2011 of GIGATL6 surface kinetic energy, integrated over the different boxes.

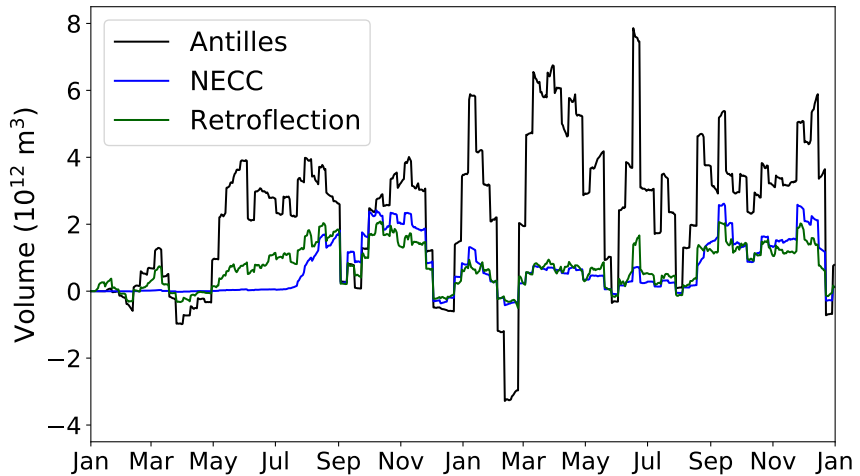


Figure 12: Lagrangian volume computed from equation (15) in the different boxes in the LAG-2D-6KM experiment (dashed lines).

in space.

LAG-2D-6KM In the Antilles, the lagrangian volume starts increasing in May. It reaches its maximum in July for both years. This corresponds to particles released when the Amazon outflow is maximum (May-June), that travel in the NBC and its rings. Most of the particles don't reach the NECC before August. The lagrangian volume reaches its maximum value in August, and then decreases slowly until the next similar event in the next year. In the retroreflection area, the lagrangian volume seems to increase at every time. This box is the only one containing land. In a 2D experiment, particles can't move on the vertical. As the primitive equations solved by the model assume an incompressible flow, it subsists a divergent component. Especially at the coast, the boundary conditions can create a convergent flow. This is the case of our simulation in the retroreflection area. Particles accumulate at the coast, which creates this artefact (see figure 16 for details).

LAG-3D-6KM Both lagrangian volumes in the retroreflection and around the Antilles increase earlier than in the 2D experiment. In the Antilles, the volume mean value is ~ 3 times higher in 3D, which is due

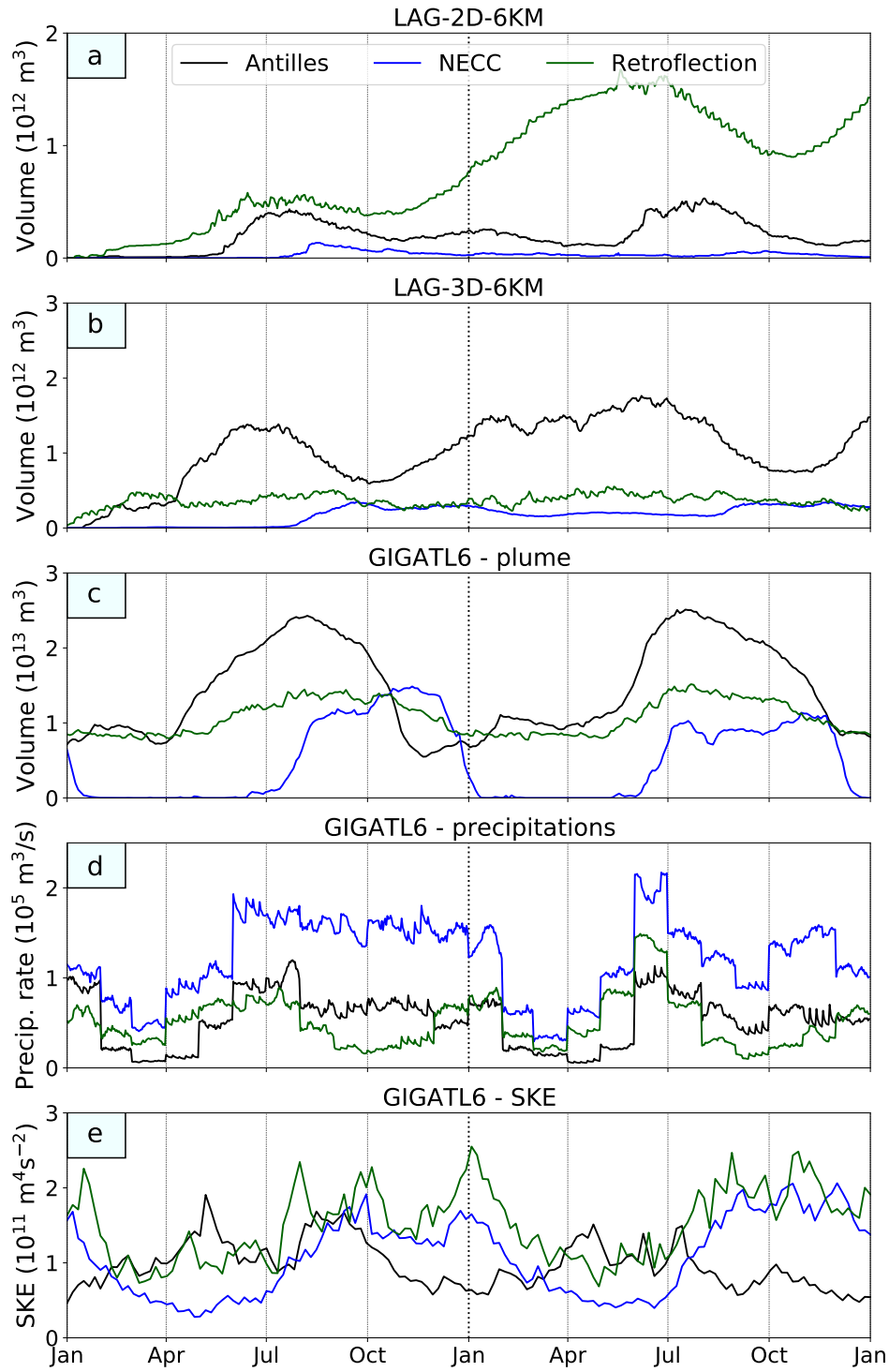


Figure 13: Lagrangian volume from 2005 to 2007 computed from equation 14 in the different boxes in the LAG-2D-6KM experiment (a), in the LAG-3D-6KM experiment (b) ; eulerian volume of fresher water than 35 psu (c) ; precipitations over the different boxes (d) ; spatially integrated SKE in the different boxes (e).

to particles that dive because of strong mixing in this region. As they are slower than in the 2D experiment, they stay a longer time in the region, so the lagrangian volume associated is large. Furthermore,

it reaches a maximum in January 2006. At the same period in 2D, the lagrangian volume is minimum, which is probably due to the same reason. In the retroflection, the volume remains approximately constant in 3D, which is more realistic. In the NECC, the summer eastward propagation is visible in August for both years with an increase of volume. More plume water seems to remain in the region, than in 2D, again because of mixing.

Thanks to these temporal series, it is also possible to give an order of magnitude of the amount of Amazon plume that propagates eastward on summer. As $\sim 10^{11} \text{m}^3$ enter the area in ~ 1 month, the mean transport towards the NECC is $\sim 0.04 \text{ Sv}$, which is 1/5 of the total discharge of the Amazon at the period where they are released.

GIGATL6 – plume First, the eulerian volume is ~ 10 times higher than the lagrangian volume. However, they still have the same order of magnitude, and it is important to notice that the eulerian and the lagrangian volumes have no reason to be more linked to each other than that, as the threshold salinity is arbitrary⁸.

In the Antilles, the eulerian volume reaches its maximum 1 month later than the lagrangian volume. As no particular meteorological event occurs, it is probably due to a weaker mixing in July. In the retroflection, it is quite constant, such as the lagrangian one in 3D. In the NECC, it starts increasing in July 2005, and does not vary much until January, which corresponds to the seasonal cycle's end of this current (see GIGATL6-SKE). It has been shown that the NECC acts as a barrier preventing mixing between the fresh water masses north of it and the salty water masses at the equator [14]. When it vanishes, mixing occurs, which makes the eulerian volume of plume decrease. In June 2006, the eulerian volume starts increasing again in the NECC, earlier than in 2005.

GIGATL6 – precipitations As the ITCZ is moving (see section 2.5), precipitations also have a seasonal cycle. They start increasing in spring until autumn. In the NECC, it is clear that the increase of eulerian volume of plume is linked to the beginning of the tropical rains, but it is not the only factor. In June 2005, the eulerian volume doesn't increase much despite the precipitations that almost doubled. The Amazon plume seems to be what triggers the freshening of water at this period. But in 2006, the eulerian volume increases mostly in June, although no plume water masses has entered the area. Then, precipitations seem to dominate the plume propagation in 2006.

GIGATL6 - SKE SKE reaches its maximum in January, only a few days after the fall of the eulerian volume. This peak corresponds to the arrival of large equatorial eddies, which mix the NECC. Since the salinity front vanishes, the jet it generates disappears, and the NECC (see section 2.3) loses intensity. The SKE reaches a maximum when a ring is in the region. The time between a maximum of the green line and a maximum of the black line corresponds to the travel of a ring. But in October of both years, SKE reaches a maximum in the retroflection, but it decreases during the whole autumn in the Antilles. It has to be related to the mixing in the Antilles region. The eulerian volume decreases the most in autumn, but not the lagrangian one (in 3D), which is characteristic of mixing. SKE doesn't reach the Antilles region as it is dissipated by turbulent mixing processes. These four different trends show together that the strongest mixing of the plume occurs in autumn because of NBC rings and instabilities generated by their passage.

5 Conclusion

5.1 Summary

It has been shown that the Amazon plume has important seasonal variations. Because of the ITCZ movements, the Amazon outflow varies, but also the Ekman transport. Although the plume follows the continental slope most of the year towards the Antilles, around 1/5 of the Amazon outflow can cross the NBC retroflection and go in the NECC at the end of summer. Thanks to the Eulerian approach, these variations have been attributed to an increase of the surface kinetic energy in the region, a change in the Ekman transport, the accumulation of fresh water in spring that accelerates the retroflection in summer. However, some GIGATL results are different from observations. On figure 8, it is clear that the model underestimates the salinity in this region. This can be due to the stratification, the parametrization of diffusivity, or the local circulation. As the eulerian approach was limited to separate the influences of the different fresh water sources, postprocessing experiments with lagrangian particles have been performed.

⁸The threshold could be chosen to get the same orders of magnitude for both volumes

The 2D experiment showed limits to describe the plume extension, especially in coastal regions where a lot of particles were stuck because of the convergence of the surface flow. The 3D experiment enabled more quantitative results than the eulerian approach, and made stronger the conclusions made in this section. Although oceanography is more used to compare flux, a new approach comparing lagrangian and eulerian volumes has shown that the Amazon outflow and the precipitations are the main responsible for the ocean's freshening in the NECC. Thanks to this method, the role of each one is explicit, and it has been shown that both can dominate each other. It has also been shown that the NECC separates fresh water at the North, and salty water at the South, and at the end of the year, this current loses intensity. The plume is mixed in the NECC region because of this. In the Antilles, the NBC rings lose an important part of their kinetic energy in autumn because of strong mixing processes.

5.2 Discussion

5.2.1 Methods

Several figures of this report show comparisons between model results and measurements. These few comparisons are just the most important ones for the results presented, but they are not the only ones that have been made. The general circulation of the region is in accordance with satellite observations. Temperature-salinity diagrams, salinity/density/velocity profiles, have been compared with those of the EUREC4A campaign and other references on the NWTA. All these diagnostics are not presented in this report as no major problem has been noticed, but they show that the model seems quite robust to describe the Amazon plume and its dynamics.

Nevertheless, it is important to notice that the numerical part of this work is only based on one simulation. It is hard to evaluate the effects of resolution (thus of the small scale structures), or the influence of tides or atmospheric forcing on mixing. Control experiments are very important to differentiate coincidences from physical correlations. With more time, results could be compared to simulations with another resolution, another grid, without river discharge, without interannual variability... With such an approach, hypotheses made on the role of the Ekman transport and the salinity front on the plume seasonal cycle would be stronger.

The CROCO model has been made for open ocean. It is clear that the coastal effects are biased by the topography smoothing, despite their importance in the Amazon outflow. We even used the smoothing to make easy the initiation of particles. By using equation (15) to compute the lagrangian volume, we tried to take in account small scale variations of velocity. We expected more realistic results, but it got actually worse. The proximity with the NBC makes the region very chaotic, so the results could be very different by using a model more precise on coastal effects.

The lagrangian particles are initiated with a horizontal space of 3 km between each other. Considering the resolution of the simulation, reducing this space would probably be dishonest, especially with a non realistic topography. Moreover, it increases the computing time, especially for some diagnostics that can be long to make. As the internship was short, it has been decided to simplify experiments to test more configurations. Concerning the time between each release, one week may seem quite a long time. Each particle represents a volume which is far shorter on the y and z -directions than on the x -direction. Indeed, if we consider currents of $\sim 0.3 \text{ m s}^{-1}$ (typical velocity at the delta), water masses of the Amazon can cross $\sim 200 \text{ km}$ in one week. A daily frequency seems then more adapted for what we aim, but results gotten with such a frequency were surprisingly really close from the weekly frequency. The choice of the initiation has been made according to these considerations.

5.2.2 Results

In the eulerian approach, every result is a mean over at least 7 years of simulation. Interannual variability is not studied in this report but it can be very important, particularly in equatorial regions, where ENSO can reverse the heat balance of the equatorial ocean. But the interannual changes due to ENSO are not as important in the Atlantic as in the Pacific, so it has been chosen to study only the seasonal variability of the region.

The choice of the boxes location is arbitrary, and one can notice that the NECC and the retroflection boxes intersect each other. This choice can be discussed as temporal series show most of the time the same features for both boxes. Nevertheless, because the retroflection is not completely stationary, it is difficult to reduce the "R" box. Similarly, the "NECC" box is hard to reduce on the western side as it is where most of the plume stops progressing.

To improve the temporal series readability, particles stuck at the coast in the 2D experiment could be removed from the diagnostics. As the retroflection was not the most important region for this experiment,

it has been chosen not to concentrate on this filtering work.

The precipitation rates presented in figure 13d are discontinuous from one month to another. It has of course no physical explanation. This data has been used at the end of the internship, and we ran out of time to completely understand why there were such gaps between months. It could be attributed to a lack of measurements in the regions, so reanalysis data is essentially based on models results, which may not be directly correlated. But of course, a mistake of our own can't be excluded.

5.3 Perspectives

More things could be done to make our conclusions stronger. For example, an idealised experiment with an eddy interacting with a salinity front could show if the retroflection acceleration is more due to the wind stress or to the Amazon outflow.

Coles *et al.* [14] made the same kind of lagrangian experiments, but with a control experiment without river discharge. With the GIGATL experiments, such an approach would be brand-new to study the role of Amazon plumes in submesoscale structures. Moreover, this work was based on the results of GIGATL6, but a similar simulation with a resolution of 1km has been performed, and its results were not available during the internship. Differences between the two simulations could show the importance of submesoscale structures for transporting and mixing the plume.

Tidal currents can exceed 2 m s^{-1} in this region, so they can be very important for vertical mixing. A similar simulation has been performed with tides but it has not been studied in this work. Compare results of both simulations would give precise results on the role of tides, especially near the coast where currents can be strong, and where most of the plume extends.

The role of NBC rings and other eddies is not an important part of this work, but they are with no doubt very important in the dynamics of the plume. Relating this report with Loïc Eisenring's would be a really interesting way to explore.

References

- [1] Aiguo Dai and Kevin E. Trenberth. "Estimates of Freshwater Discharge from Continents: Latitudinal and Seasonal Variations in: Journal of Hydrometeorology Volume 3 Issue 6 (2002)". In: *Journal of Hydrometeorology* (2002). DOI: https://journals.ametsoc.org/search?f_0=author&q_0=Kevin+E.+Trenberth. URL: https://journals.ametsoc.org/view/journals/hydr/3/6/1525-7541_2002_003_0660_eofdfc_2_0_co_2.xml.
- [2] S Masson and P Delecluse. "Influence of the Amazon River runoff on the tropical atlantic". In: *Physics and Chemistry of the Earth, Part B: Hydrology, Oceans and Atmosphere* 26.2 (Jan. 1, 2001), pp. 137–142. ISSN: 1464-1909. DOI: 10.1016/S1464-1909(00)00230-6. URL: <https://www.sciencedirect.com/science/article/pii/S1464190900002306>.
- [3] Ilson C. A. da Silveira, Luiz B. de Miranda, and Wendell S. Brown. "On the origins of the North Brazil Current". In: *Journal of Geophysical Research: Oceans* 99 (C11 1994), pp. 22501–22512. ISSN: 2156-2202. DOI: 10.1029/94JC01776. URL: <https://agupubs.onlinelibrary.wiley.com/doi/abs/10.1029/94JC01776>.
- [4] D. M. Fratantoni, W. E. Johns, and T. L. Townsend. "Rings of the North Brazil Current: their structure and behavior inferred from observations and a numerical simulation". In: *Journal of Geophysical Research* 100 (C6 1995), pp. 10, 633–10, 654. ISSN: 0148-0227. DOI: 10.1029/95jc00925. URL: <https://miami.pure.elsevier.com/en/publications/rings-of-the-north-brazil-current-their-structure-and-behavior-in>.
- [5] L. C. Aroucha et al. "Intra- and Inter-Annual Variability of North Brazil Current Rings Using Angular Momentum Eddy Detection and Tracking Algorithm: Observations From 1993 to 2016". In: *Journal of Geophysical Research: Oceans* 125.12 (Dec. 2020). ISSN: 2169-9275, 2169-9291. DOI: 10.1029/2019JC015921. URL: <https://onlinelibrary.wiley.com/doi/10.1029/2019JC015921>.
- [6] Moacyr Araujo, Carlos Noriega, and Nathalie Lefèvre. "Nutrients and carbon fluxes in the estuaries of major rivers flowing into the tropical Atlantic". In: *Frontiers in Marine Science* 1 (May 2014). Publisher: Frontiers Media, p. 10. DOI: 10.3389/fmars.2014.00010. URL: <https://hal.archives-ouvertes.fr/hal-01375592>.
- [7] W. Douglas Wilson, William E. Johns, and Silvia L. Garzoli. "Velocity structure of North Brazil Current rings". In: *Geophysical Research Letters* 29.8 (2002), pp. 114–1–114–4. ISSN: 1944-8007. DOI: 10.1029/2001GL013869. URL: <https://agupubs.onlinelibrary.wiley.com/doi/abs/10.1029/2001GL013869>.

- [8] David M. Fratantoni and Philip L. Richardson. "The Evolution and Demise of North Brazil Current Rings". In: *Journal of Physical Oceanography* 36.7 (July 1, 2006). Publisher: American Meteorological Society Section: Journal of Physical Oceanography, pp. 1241–1264. ISSN: 0022-3670, 1520-0485. DOI: 10.1175/JPO2907.1. URL: <https://journals.ametsoc.org/view/journals/phoc/36/7/jpo2907.1.xml>.
- [9] K. Alapati and S. Raman. "A study of the seasonal migration of ITCZ and the quasi-periodic oscillations in a simple monsoon system using an energy balance model". In: *Meteorology and Atmospheric Physics* 41.4 (Dec. 1, 1989), pp. 191–211. ISSN: 1436-5065. DOI: 10.1007/BF01026110. URL: <https://doi.org/10.1007/BF01026110>.
- [10] David M. Fratantoni and Deborah A. Glickson. "North Brazil Current Ring Generation and Evolution Observed with SeaWiFS". In: *Journal of Physical Oceanography* 32.3 (Mar. 1, 2002). Publisher: American Meteorological Society Section: Journal of Physical Oceanography, pp. 1058–1074. ISSN: 0022-3670, 1520-0485. DOI: 10.1175/1520-0485(2002)032<1058:NBCRGA>2.0.CO;2. URL: https://journals.ametsoc.org/view/journals/phoc/32/3/1520-0485_2002_032_1058_nbcrga_2.0.co_2.xml.
- [11] Ning Zeng. "Seasonal cycle and interannual variability in the Amazon hydrologic cycle". In: *Journal of Geophysical Research: Atmospheres* 104 (D8 1999), pp. 9097–9106. ISSN: 2156-2202. DOI: 10.1029/1998JD200088. URL: <https://agupubs.onlinelibrary.wiley.com/doi/abs/10.1029/1998JD200088>.
- [12] Leif N. Thomas et al. "Symmetric instability in the Gulf Stream". In: *Deep Sea Research Part II: Topical Studies in Oceanography*. Subtropical Mode Water in the North Atlantic Ocean 91 (July 1, 2013), pp. 96–110. ISSN: 0967-0645. DOI: 10.1016/j.dsr2.2013.02.025. URL: <https://www.sciencedirect.com/science/article/pii/S0967064513000829>.
- [13] H. L. Varona et al. "Amazon River plume influence on Western Tropical Atlantic dynamic variability". In: *Dynamics of Atmospheres and Oceans* 85 (Mar. 1, 2019), pp. 1–15. ISSN: 0377-0265. DOI: 10.1016/j.dynatmoce.2018.10.002. URL: <https://www.sciencedirect.com/science/article/pii/S0377026517300866>.
- [14] Victoria J. Coles et al. "The pathways and properties of the Amazon River Plume in the tropical North Atlantic Ocean". In: *Journal of Geophysical Research: Oceans* 118.12 (2013). _eprint: <https://agupubs.onlinelibrary.wiley.com/doi/pdf/10.1002/2013JC008981>, pp. 6894–6913. ISSN: 2169-9291. DOI: 10.1002/2013JC008981. URL: <https://agupubs.onlinelibrary.wiley.com/doi/abs/10.1002/2013JC008981>.
- [15] Bjorn Stevens et al. "EUREC4A". In: *Earth System Science Data* 13.8 (Aug. 25, 2021). Publisher: Copernicus GmbH, pp. 4067–4119. ISSN: 1866-3508. DOI: 10.5194/essd-13-4067-2021. URL: <https://essd.copernicus.org/articles/13/4067/2021/>.
- [16] G. Reverdin et al. "Formation and Evolution of a Freshwater Plume in the Northwestern Tropical Atlantic in February 2020". In: *Journal of Geophysical Research: Oceans* 126.4 (2021). _eprint: <https://agupubs.onlinelibrary.wiley.com/doi/pdf/10.1029/2020JC016981>, e2020JC016981. ISSN: 2169-9291. DOI: 10.1029/2020JC016981. URL: <https://agupubs.onlinelibrary.wiley.com/doi/abs/10.1029/2020JC016981>.
- [17] P. L. Richardson and G. Reverdin. "Seasonal cycle of velocity in the Atlantic North Equatorial Countercurrent as measured by surface drifters, current meters, and ship drifts". In: *Journal of Geophysical Research: Oceans* 92 (C4 1987), pp. 3691–3708. ISSN: 2156-2202. DOI: 10.1029/JC092iC04p03691. URL: <https://agupubs.onlinelibrary.wiley.com/doi/abs/10.1029/JC092iC04p03691>.
- [18] Iwona Wróbel-Niedźwiecka, Violetta Drozdowska, and Jacek Piskozub. "Effect of drag coefficient formula choice on wind stress climatology in the North Atlantic and the European Arctic". In: *Oceanologia* 61.3 (July 1, 2019), pp. 291–299. ISSN: 0078-3234. DOI: 10.1016/j.oceano.2019.02.002. URL: <https://www.sciencedirect.com/science/article/pii/S0078323419300235>.

Annexes

Sigma coordinates

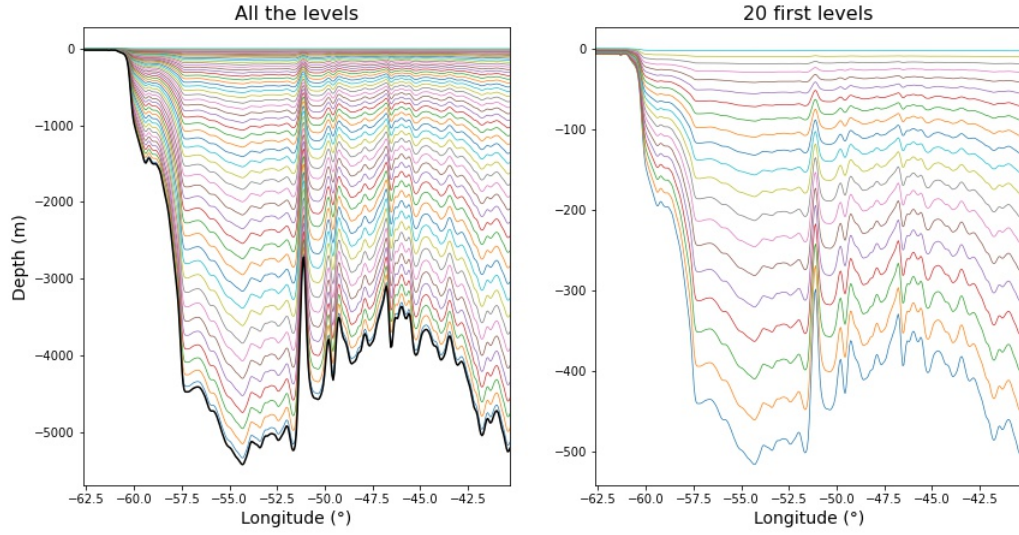


Figure 14: Illustration of sigma levels for a zonal section. Thick line represents the ocean bottom, colored lines represent the sigma levels. Levels are more concentrated in the upper layer, as it is where the strongest dynamical events occur (intense currents, mixing due to instabilities).

Surface currents anomaly

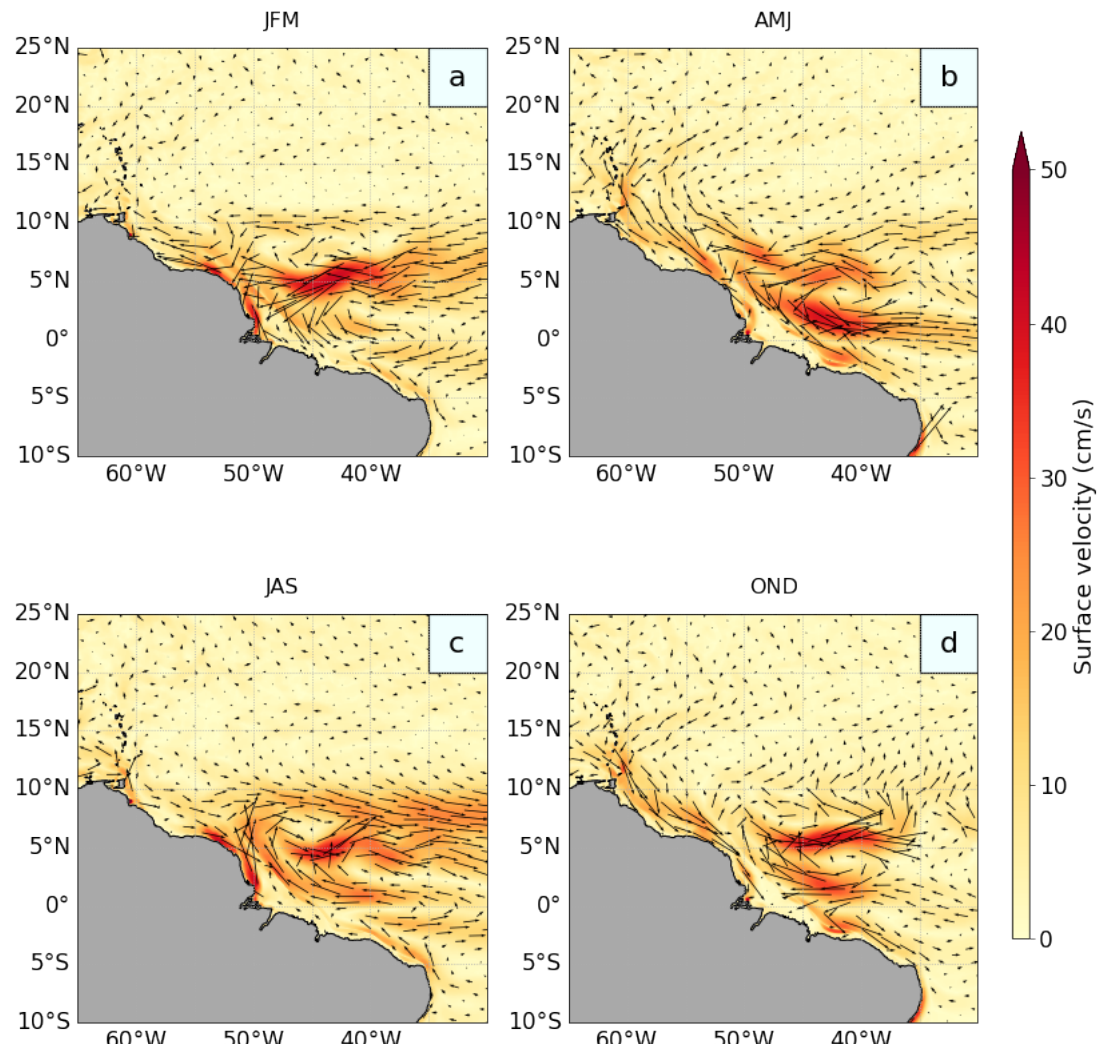


Figure 15: GIGATL6 mean surface currents anomaly over 8 years.

Vertical velocity in the retroflection region

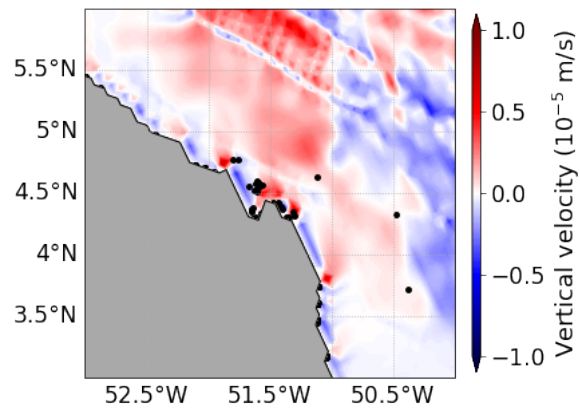


Figure 16: Mean vertical velocity in the retroflection area. Black dots are the particles at a random instant. 3D particles can dive and move offshore even close to the coast, but surface particles keep being brought back to the coast line.